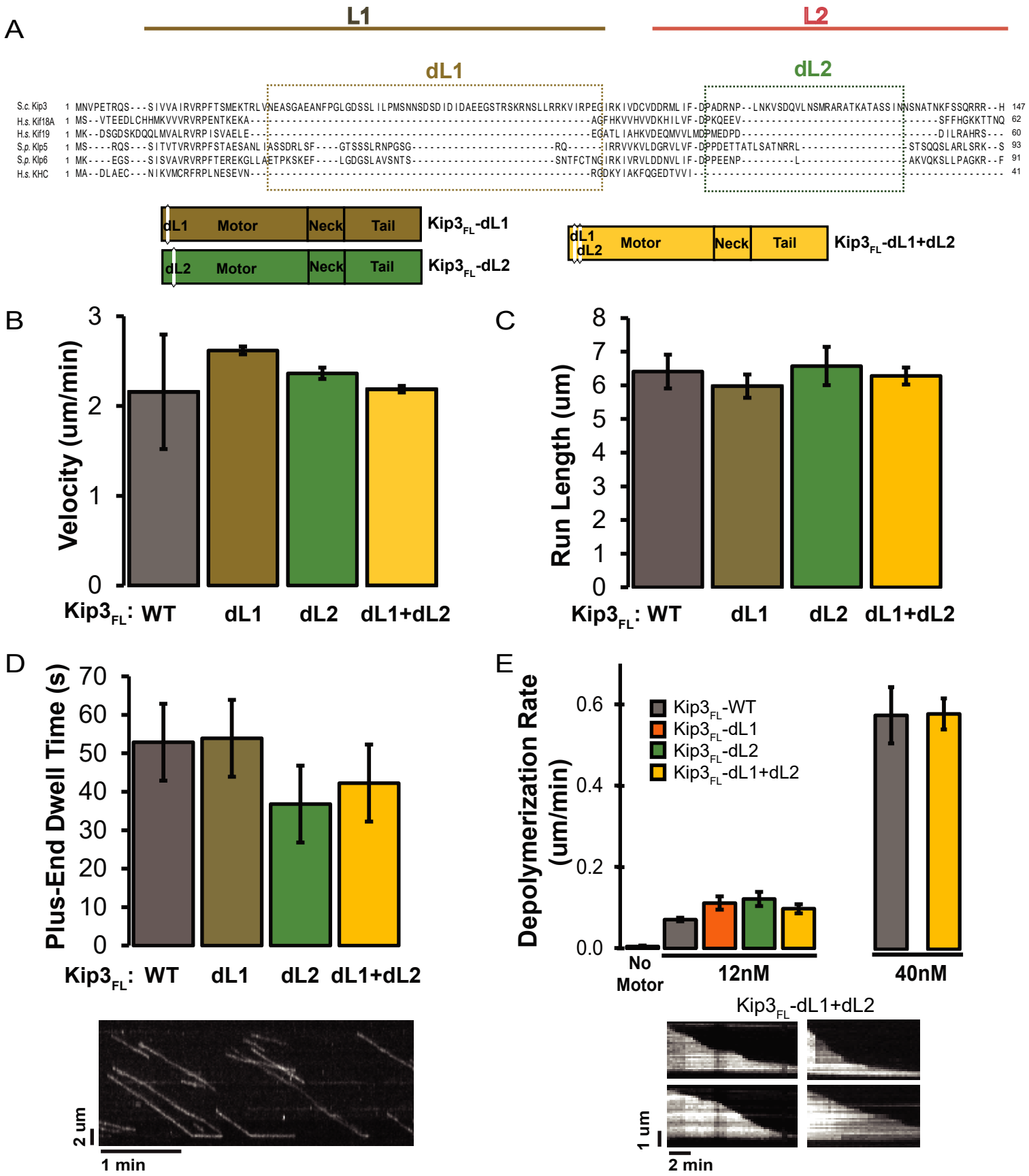
A
L1
L2
dL1
dL2
S.c. Kip3
H.s. Kif18A
H.s. Kif19
S.p. Klp5
S.p. Klp6
H.s. KHC
dL1 Motor Neck Tail
Kip3FL-dL1
dL2 Motor Neck Tail
Kip3FL-dL2
dL1 dL2 Motor Neck Tail
Kip3FL-dL1+dL2
B
Velocity (um/min)
Kip3FL: WT dL1 dL2 dL1+dL2
C
Run Length (um)
Kip3FL: WT dL1 dL2 dL1+dL2
D
Plus-End Dwell Time (s)
Kip3FL: WT dL1 dL2 dL1+dL2
2 um
1 min
E
Depolymerization Rate (um/min)
Kip3FL-WT
Kip3FL-dL1
Kip3FL-dL2
Kip3FL-dL1+dL2
No Motor
12nM
40nM
Kip3FL-dL1+dL2
1 um
2 min

Fig. S1

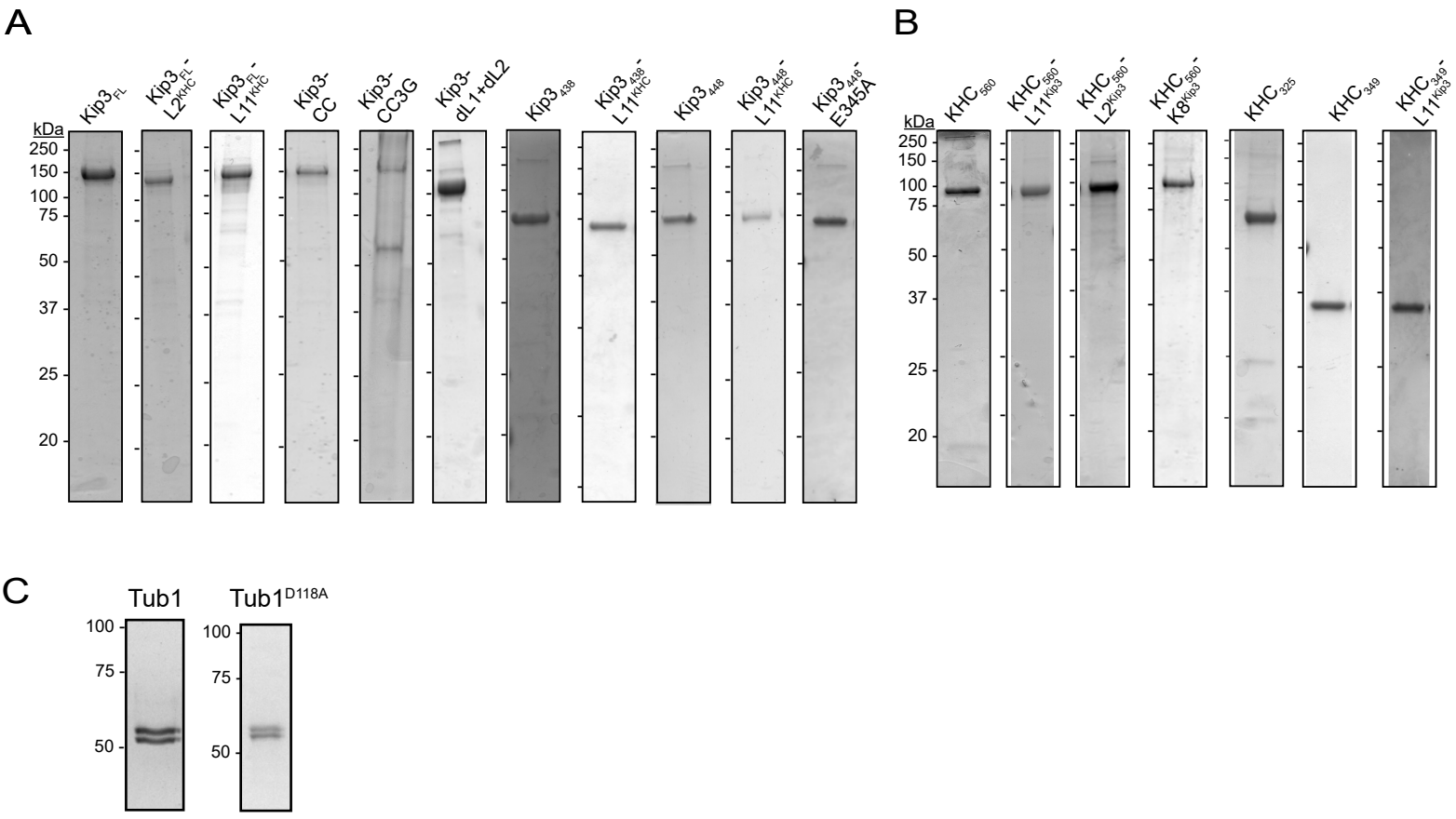
A
kDa
250
150
100
75
50
37
25
20
Kip3FL
Kip3FL - L2KHC
Kip3FL - L11KHC
Kip3-CC
Kip3-CC3G
Kip3-dL1+dL2
Kip3438
Kip3438 - L11KHC
Kip3448
Kip3448 - L11KHC
Kip3448 - E345A
B
kDa
250
150
100
75
50
37
25
20
KHC560
KHC560 - L11Kip3
KHC560 - L2Kip3
KHC560 - K8Kip3
KHC325
KHC349
KHC349 - L11Kip3

C
Tub1
Tub1D118A
100
75
50
100
75
50

Fig. S2

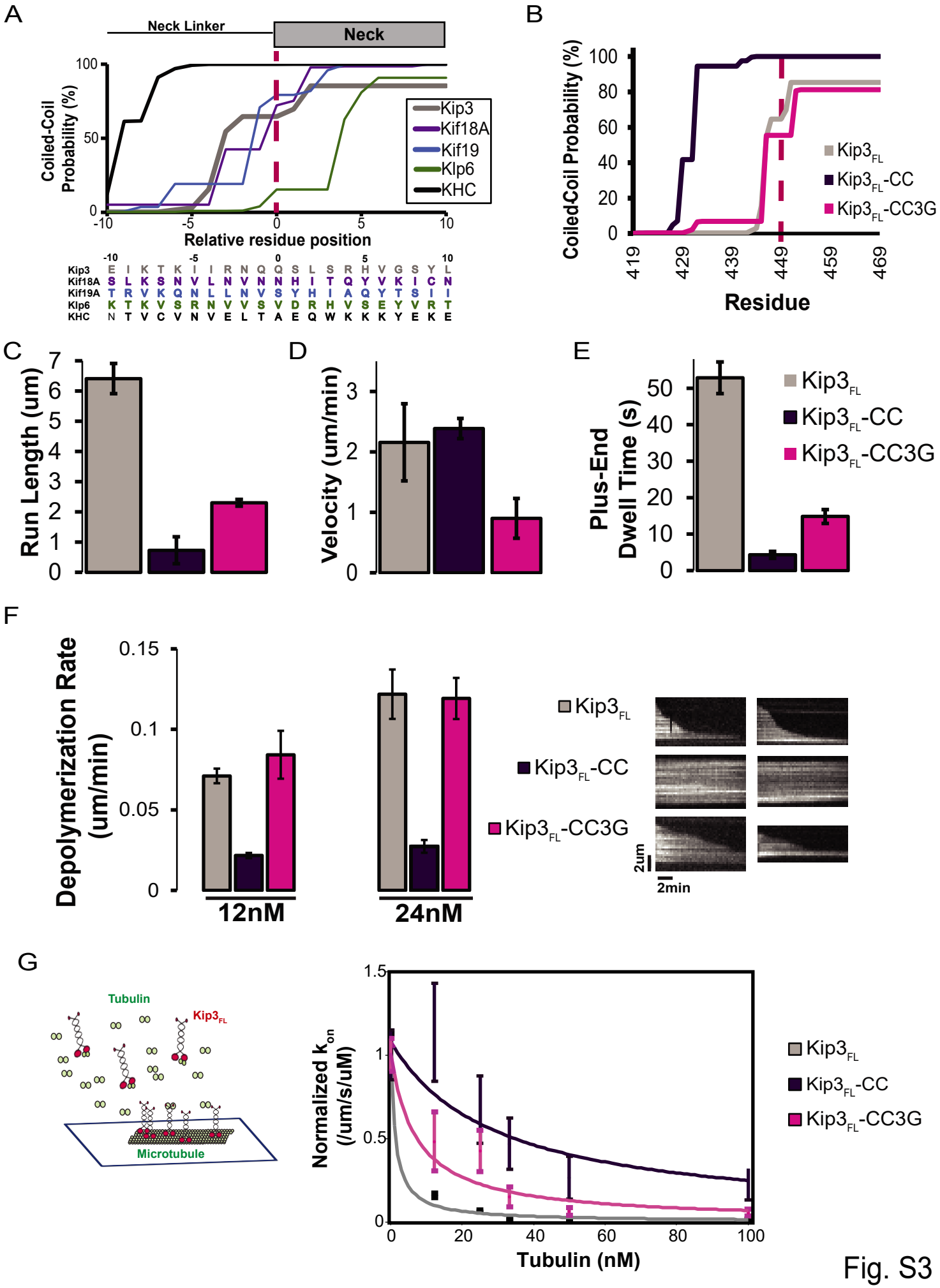
A
Neck Linker
Neck
Coiled-Coil Probability (%)
Relative residue position
Kip3
Kif18A
Kif19
Klp6
KHC
B
CoiledCoil Probability (%)
Residue
Kip3FL
Kip3FL-CC
Kip3FL-CC3G
C
Run Length (um)
D
Velocity (um/min)
E
Plus-End Dwell Time (s)
F
Depolymerization Rate (um/min)
12nM
24nM
2um
2min
G
Tubulin
Kip3FL
Microtubule
Normalized kon (/um/s/uM)
Tubulin (nM)

Fig. S3

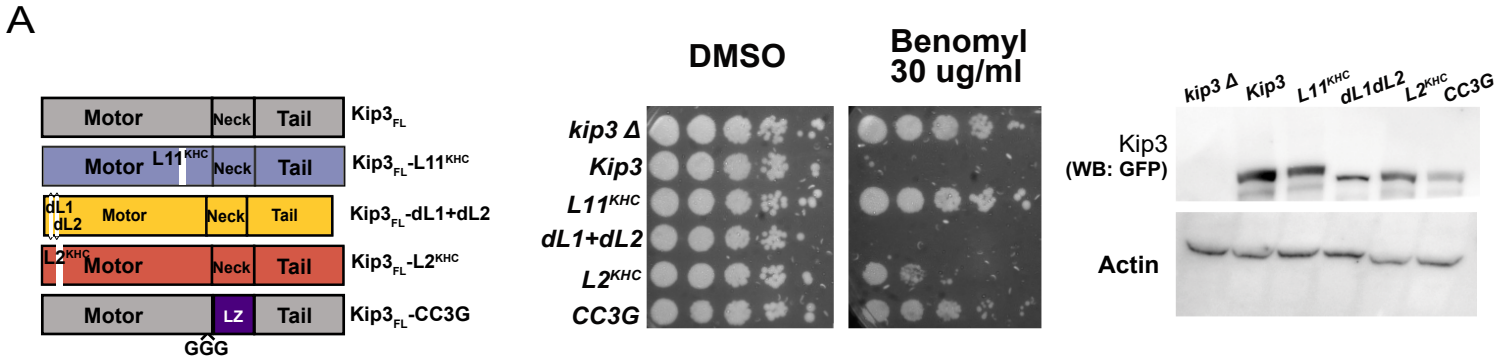

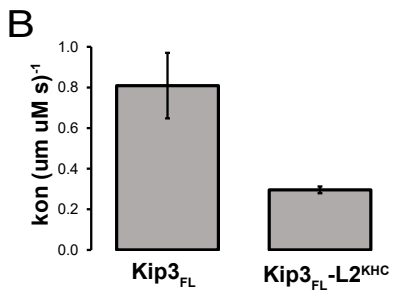

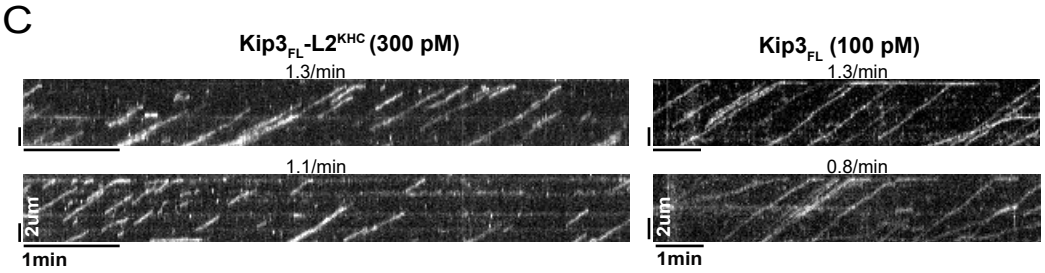

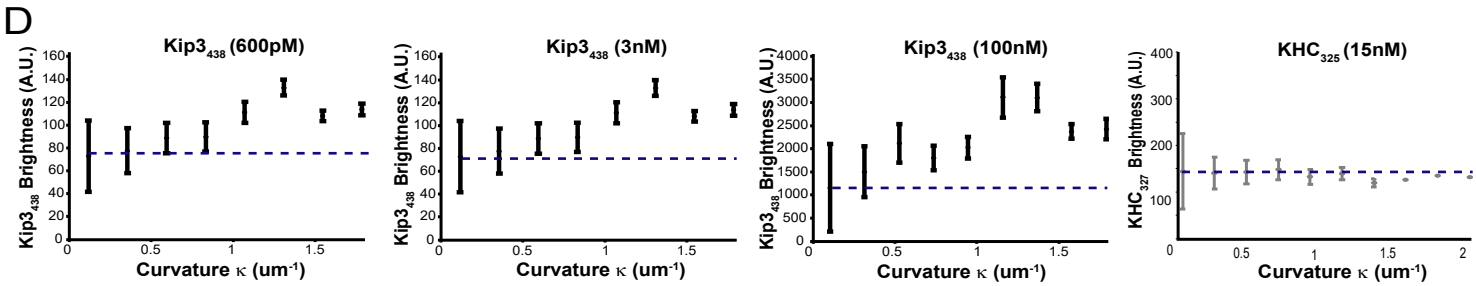

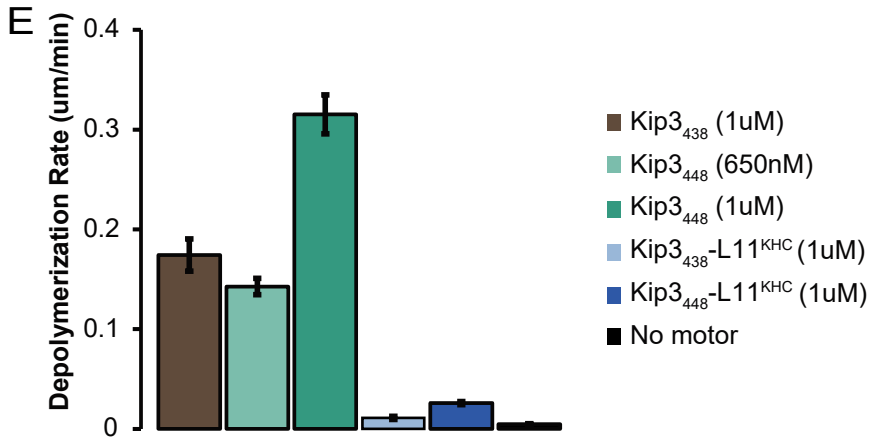

F

	Tubulin			
	K_D (uM)	+/- (uM)	k_{off} (s^{-1})	+/- (s^{-1})
$Kip3_{438}$	0.06	0.02	0.018	0.002
$Kip3_{438}$-$L11^{KHC}$	0.44	0.16	0.111	0.005
$Kip3_{448}$	0.05	0.01	0.021	0.005
$Kip3_{448}$ (ADP)	0.18	0.02	0.028	0.001
$Kip3_{448}$-$L11^{KHC}$	0.28	0.02	S.S.	S.S.

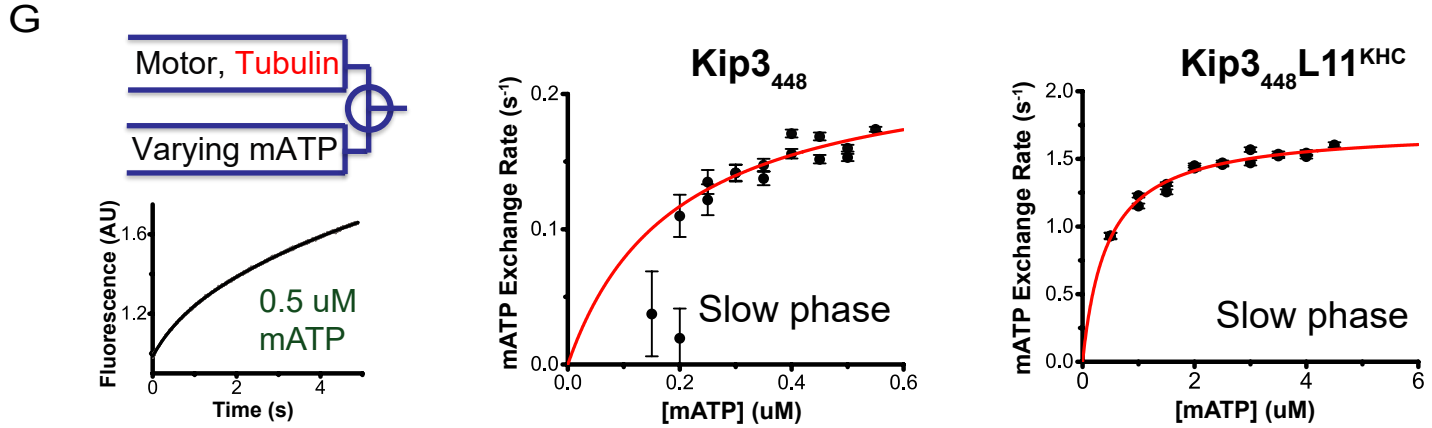

Fig. S4

A

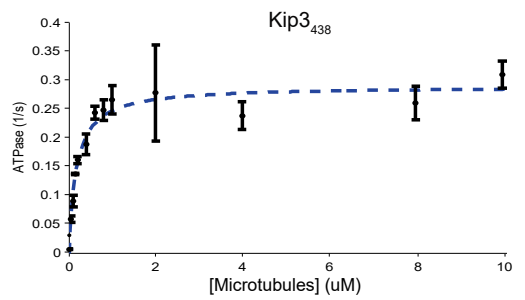

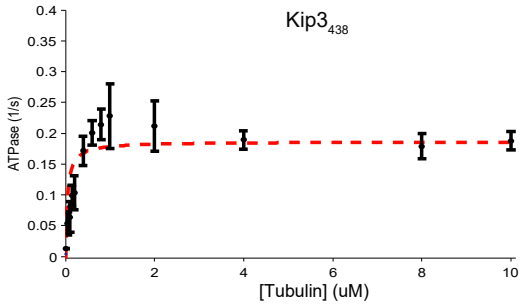

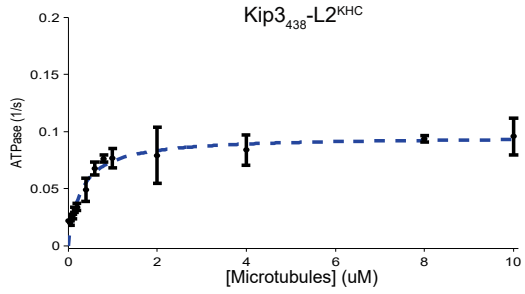

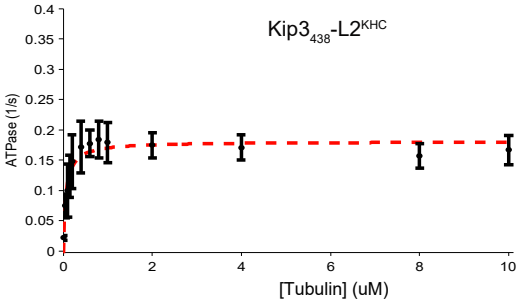

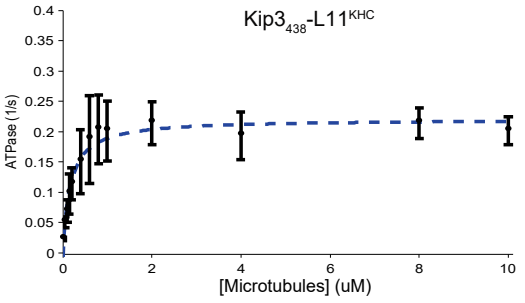

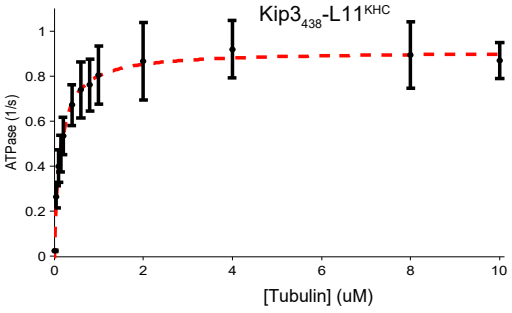

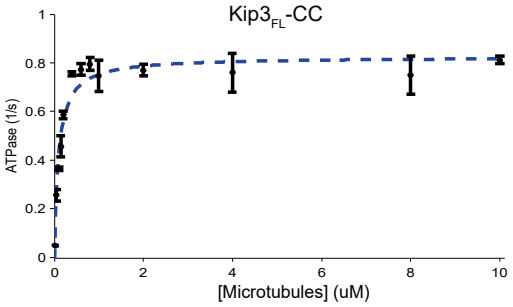

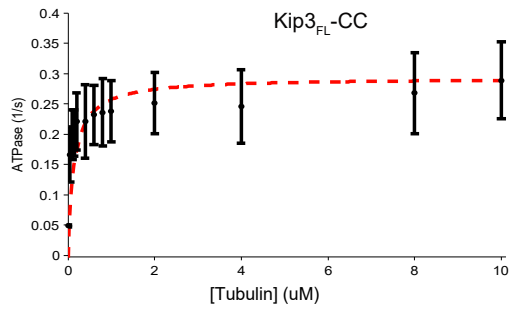

B

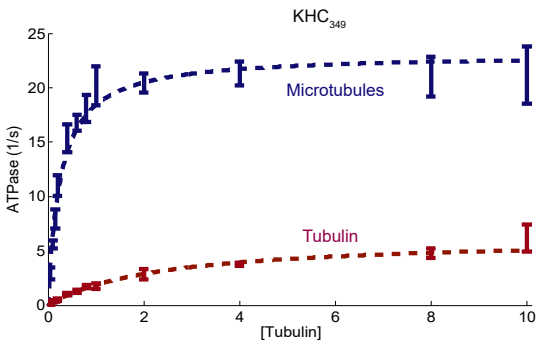

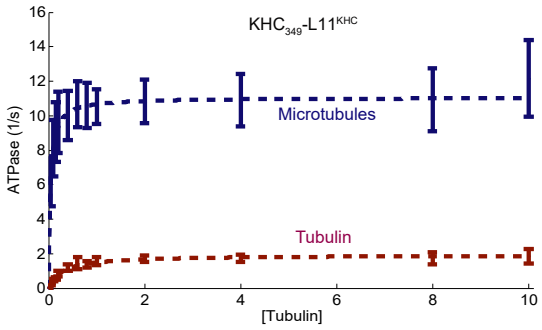

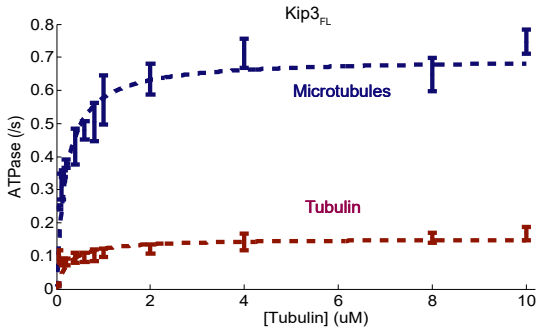

C

Steady State ATPase KHC Constructs

	Microtubule		Tubulin	
	K_M (uM)	k_{cat} (s^{-1})	K_M (uM)	k_{cat} (s^{-1})
KHC_{349}	0.231 +/- 0.026	22.67 +/- 0.94	2.44 +/- 0.31	6.29 +/- 0.46
KHC_{349}-$Kip3^{L11}$	0.041 +/- 0.005	11.25 +/- 0.85	0.260 +/- 0.011	1.89 +/- 0.19

Fig. S5

SUPPLEMENTAL FIGURE LEGENDS

Figure S1. *Sacharomyces cerevisiae*-specific insertions in Loop1 and Loop2 are not required for motility or depolymerization activity. Related to Figure 1, 4-6.

A. Alignment of protein sequences of kinesin-8 family members and KHC. Kip3-specific Loop1 (dL1:aa 30-85) or Loop2 (dL2:aa 106-134) insertions are shown within the brown or green dashed boxes. These Kip3-specific sequences were deleted and denoted as dL1 and dL2. **Bottom:** diagram of the relevant constructs.

   B-D. Single molecule motility of $Kip3_{FL}$, $Kip3_{FL}$-dL1, $Kip3_{FL}$-dL2 or $Kip3_{FL}$-dL1+dL2 (dL1+dL2) constructs assayed by TIRF microscopy on taxol-stabilized microtubules: **B.** Velocity. **C.** Run length and **D.** Plus-end dwell time (mean +/- SEM; n=75-214 events). **D, bottom**: kymograph showing the motility and plus-end residence of Kip3-dL1-dL2 on taxol stabilized microtubules. Scale bar: 2um (vertical), 1min (horizontal).

E. Quantification of the depolymerization rates of GMPCPP-stabilized microtubules after addition of the $Kip3_{FL}$-dL1 and $Kip3_{FL}$-dL2 deletion constructs (mean +/- SEM; n_{MT}=45-242). **Bottom:** kymographs from depolymerase assays on GMPCPP-stabilized microtubules with $Kip3_{FL}$-dL1+dL2; 40nM input. Scale bar: 1um (vertical), 2 min (horizontal).

Figure S2. Purification of Kip3 variants. Related to Figure 1-6.

A. Coomassie-stained SDS-PAGE gels of representative $Kip3_{FL}$ and Kip3 variant purifications.
B. Coomassie-stained SDS-PAGE gels of representative KHC_{560} and KHC variant purifications.
C. Coomassie-stained SDS-PAGE gels of representative Tub1 and $Tub1^{D118A}$ purifications.

Figure S3. A flexible segment on the N-terminus of the neck is required for depolymerization by dimeric Kip3. Related to Figure 3.

A. Kinesin-8s have a unique neck architecture. Probability of forming a coiled-coil (MARCOIL) for various kinesin-8s at the base of the neck. The start of the first residue of the neck has been placed as the x-axis origin. Top: Cartoon illustrating the beginning of the neck at the "0" residue position. Bottom: sequence alignment of the beginning of the neck region for the kinesin-8s shown in the graph. Other kinesin-8s were omitted for clarity. Similar results were obtained with PCOILS and COILS.

B. Probability of forming a coiled-coil (MARCOIL) for $Kip3_{FL}$ and neck mutants. $Kip3_{FL}$ is shown in grey; Kip3 'coiled-coiled' ($Kip3_{FL}$-CC, purple) has its native neck replaced by a leucine zipper as described in (Su et al. 2013); $Kip3_{FL}$-CC3G (mexican pink) contains a 3 glycine insertion at the base of the leucine-zipper neck (450). The $Kip3_{FL}$-CC3G mutant was engineered to have a coiled-coil probability similar to $Kip3_{FL}$.

C. D. E. Quantification of the motility of the neck mutants under single molecule conditions, imaged by TIRF microscopy on taxol-stabilized microtubules: **C.** Run Length; **D.** Velocity (mean +/- n=155-430 events); **E.** Plus-end dwell time (mean +/- SEM; n=26-149 events). Note that the assays shown here were performed at 100 mM KCl. At an ionic concentration of 50 mM KCl the motility of $Kip3_{FL}$-CC's is comparable to $Kip3_{FL}$ (Su et al. 2013)

F. A unique neck architecture is required for Kip3's depolymerization activity. Measurement of the depolymerization rate of GMPCPP-stabilized microtubules $Kip3_{FL}$ (grey), $Kip3_{FL}$-CC (purple), $Kip3_{FL}$-CC3G (Mexican pink) at 12nM and 24nM dimer (mean +/- SEM; n_{MT}=32-249). **Right:** Kymographs of GMPCPP-stabilized microtubules upon addition of Kip3 neck mutants (24nM input). Scale bar: 2 um (vertical), 2 min (horizontal).

G. The ability to bind tubulin dimers correlates with depolymerization activity. **Left:** Schematic of the tubulin competition assay. The microtubule on-rate of the relevant motor construct is measured in the presence of varying concentrations of soluble tubulin. **Right:** Single molecule on-rate for taxol-stabilized microtubules in the competition assay after addition of tubulin for $Kip3_{FL}$ (grey), $Kip3_{FL}$-CC (purple) and $Kip3_{FL}$-CC3G (mexican pink). On-rates were normalized to 0nM tubulin. Data was fit to an enzymatic competition model by an inhibitor, see methods. $Kip3_{FL}$: K_i^{APP} = 1.3 nM +/- 1.2 nM (95% CI fit, R^2=0.92; N=5-9 flow-cells per concentration, n=1836 total events); $Kip3_{FL}$-CC: K_i^{APP}=29.8 nM +/- 30nM (95% CI fit, R^2=0.84, N=4-6 flow-cells per concentration, n=4031 total events); $Kip3_{FL}$-CC3G K_i^{APP}= 7.2 nM +/- 6nM (95% CI fit, R^2=0.94, N=4-8 flow cells per concentration, n=5619 total events).

Figure S4. Characterization of Kip3 variants. Related to Figure 2, 4, 5, S1, S3.

A. In *vivo* complementation by *kip3* mutant constructs. **Left:** Diagram of Kip3 full length dimer constructs used. **Middle:** Benomyl resistance assay: Cultures expressing the indicated constructs were spotted onto plates of YPD+ 1% DMSO (LHS, control) or on YPD + 30ug/ml benomyl in 1 % DMSO to assay for resistance to the microtubule depolymerizing drug benomyl. Wild-type strains are benomyl sensitive whereas the deletion allele, *kip3*Δ*,* is benomyl resistant**. Right**: Control western blot for strains used in benomyl resistance assay. Actin was used as a loading control. Kip3-GFP and other constructs steady-state levels were detected with an anti-GFP antibody.

B. Kip3 L2 increases the microtubule-on rate of the motor. Single molecule microtubule on-rate (k_{on}) for $Kip3_{FL}$ and $Kip3_{FL}$-$L2^{KHC}$ measured with TIRF microscopy on taxol-stabilized microtubules (mean +/- SEM; n=673-913 events).

C. Kymographs illustrating the normalized flux of motors to the plus-end for $Kip3_{FL}$ and $Kip3_{FL}$-$L2^{KHC}$ imaged by TIRF microscopy. $Kip3_{FL}$ was introduced at 100pM and $Kip3_{FL}$-$L2^{KHC}$ at 300pM. See methods for details. Scale bar: 1 min (horizontal), 2 um (vertical).

D. Kip3 binds preferentially to curved regions of flow-bent microtubules. Taxol-stabilized microtubules were bent under flow, labelled $Kip3_{438}$ was introduced into the flow chamber and imaged under TIRF microscopy. Integrated $Kip3_{438}$ intensity was plotted against the absolute curvature (κ) of the microtubule (mean +/- SE) at 600pM, 3nM and 100nM input respectively (n_{MT}=139, 52, 61 respectively). KHC_{325} at 15nM input is shown as a control (n_{MT}=165). A line with a slope of 0 has been drawn as a visual reference.

E. $Kip3_{448}$ depolymerizes GMPCPP-stabilized microtubules similarly to $Kip3_{438}$ and like dimeric Kip3-$L11^{KHC}$ (Fig. 2D), $Kip3_{448}$-$L11^{KHC}$ lacks depolymerase activity. Quantification of the depolymerization rate (GMPCPP-microtubules) of $Kip3_{438}$, $Kip3_{448}$, $Kip3_{438}$-$L11^{KHC}$, $Kip3_{448}$-$L11^{KHC}$ and the no motor control. Shown are mean +/- SEM (n_{MT}=100-298).

F. Affinity and off-rate measurements of the binding of tubulin to immobilized monomeric Kip3 constructs using bio-layer interferometry. All assays were performed in ATP unless stated in the table. Shown are mean +/- SEM (n=14-30 concentrations per condition). SS: measured using steady state values.

G. Tubulin does not interfere with ATP binding to Kip3. Tubulin-incubated $Kip3_{448}$ was rapidly mixed with varying concentrations of mantATP**. Left, top:** schematic of the experiment**. Left, bottom:** representative trace upon mixing of motor-tubulin complex and mantATP. A bi-exponential signal can be observed with two distinct phases. The initial fast phase reflects the initial binding of mantATP to the Kip3448-tubulin complex and is reported in Figure 5F. The second, slow phase (shown here) is inferred to correspond to the post-hydrolysis mantATP exchange after ADP release from a

tubulin-bound ADP-motor. Slow phase of the bi-exponential signal is plotted for $Kip3_{448}$ (middle) and $Kip3_{448}$-$L11^{KHC}$ (right). Shown are mean +/- SEM; N=5-6 per point.

Figure S5. Steady state ATPase assays for Kip3 constructs. Related to Figure 4, 5.

A. Steady state ATPase assays with monomeric $Kip34_{348}$ variants and $Kip3_{FL}$-CC. Left: Microtubule-stimulated (left, blue traces) or tubulin-stimulated (right, red traces) ATPase activity (mean +/- SEM; n=3-4 curves per condition). Dashed lines represent weighted fits to the Michaelis-Menten equation. ATPase rates are shown in Fig. 4D.
B. Steady state ATPase assays with dimeric $Kip3_{FL}$, KHC_{349} and KHC_{349}-$L11^{KHC}$ on microtubules (blue) or free tubulin (red) as substrate (0-10 uM). Shown are the ATPase rates (1/s, mean +/- SEM; n=3-4 curves per condition). Dashed lines represent weighted fits to the Michaelis-Menten equation. Binding of KHC_{349} to MTs is salt sensitive, therefore these assays were conducted without added salt, see methods.
C. Values from steady state ATPase assays with KHC_{349} and KHC_{349}-$Kip3^{L11}$ constructs on microtubules or free tubulin as substrate. ATPase assays with KHC_{349} were conducted without added salt, see methods. Shown are mean +/- SEM; n=3-4 curves per condition.